Chapter 15
Template Assisted Formation of Metal Nanotubes

Ion Tiginyanu, Veaceslav Ursaki and Eduard Monaico

Abstract This chapter provides a review of methods for the production of metal nanotubes and their applications. The importance of nanotemplated growth of nanowires and nanotubes for nanofabrication, and the advantages of nanotubes over nanowires are revealed. Technological approaches for producing various templates, as well as advantages and drawbacks of specific templates, such as ion-track membranes, porous alumina templates, and porous semiconductor templates for nanofabrication are discussed, especially with respect to their suitability for the production of metal nanotubes. Technological methods applied for deposition of metal nanotubes with a focus on electrodepostion and electroless deposition are overviewed for each type of porous templates, and their mechanisms and peculiarities are evidenced. The prospects of application of nanomaterials based on porous nanotemplates in electronics, energy sector, optics, photonics, computers and communications, magnetism and biomedical sciences are explored.

15.1 Introduction

A wide field of potential applications, ranging from electronics, computers and communications to life sciences and biotechnology relies nowadays on the synthesis of functional nanoscale materials and devices. On the other hand, technological development in this area requires wide and intensive research, particularly in miniaturization and preparation of materials with low dimensionality and investigation of their properties which differ strongly from those of bulk materials. The

I. Tiginyanu · V. Ursaki (✉)
Institute of Electronic Engineering and Nanotechnologies "D. Ghitu",
Academy of Sciences of Moldova, Chisinau, Moldova
e-mail: ursaki@yahoo.com

I. Tiginyanu · E. Monaico
National Center for Materials Study and Testing, Technical University of Moldova,
Chisinau, Moldova

strong change in properties of nanoscale materials and devices is induced by the low dimensionality and high surface to volume ratio.

Nanotemplates are widely used in nanofabrication, particularly in the production of large assembles of nanowires and nanotubes of various materials with defined shapes and dimensions [1–4].

Due to their unique properties, metal nanowires and nanotubes, as well as 2D metallo-semiconductor interpenetrating networks are promising for various nano-electronic and optoelectronic applications. Nanowires are used in nanoelectronic devices as interconnects, transparent and flexible electrodes, magnetic devices, chemical and biological sensors [5–10]. The optoelectronic applications of metallic nanowires and nanotubes are based on the extended dielectric/metal interface that can sustain the propagation of electromagnetic waves coupled to collective oscillations of the conduction electrons in the metal, the so called surface plasmon polaritons, allowing the manipulation and transmission of light on the nanoscale [11, 12]. 2D metallo-semiconductor networks are particularly used in sensors involving barrier structures and plasmonic excitations and memory media based on magnetic nanostructures embedded in semiconductor matrices [13–15].

Metallic [2, 3, 16–19] or semiconductor [20–23] nanowires or nanotubes with aspect ratios exceeding sometimes 1000 have been produced by employing the nanotemplate approach.

15.2 Porous Templates for Nanofabrication

Over the last decade, different template-based nanofabrication approaches have been developed which offer the possibility to produce large assembles of nanowires and nanotubes of various materials with defined diameters and lengths [1, 24–28]. Nowadays two types of templates are widely used for nanofabrication purposes, namely porous Al_2O_3 and etched ion track membranes based either on inorganic materials or on organic polymers [25–28]. Both porous Al_2O_3 and etched ion track membranes, however, exhibit high resistivity and therefore they often play a passive role in nanofabrication processes. In particular, templated growth of nanowires via electroplating is provided usually by the metal contact deposited on the back side of the high-resistivity membranes, while electroplating of metal nanotubes requires additional technological steps e.g. chemical modification of the inner surface of the pores prior to electrodeposition which leads to the incorporation of spurious phases in the nanotube walls [26]. Semiconductor nanotemplates which properties can be easily controlled by external illumination, applied electric fields, etc. provide wider possibilities for nanofabrication.

The etched ion track membranes are produced by bombarding thin polymeric films with heavy energetic ions (with specific energies higher than 1 MeV/nucleon) provided, for example, by a cyclotron, followed by chemical etching, which removes the weakened zones with chemical bonds damaged by the heavy ion bombardment. Each ion passing through the polymer foil produces a track, a

cylindrical zone of material with altered properties, which leads to the decomposition of the polymer material. At the step of chemical etching one has to choose carefully the composition of the etching bath and the temperature at which the etching is performed in order to produce pores with the desired shape and size.

The shape and size of the pore are determined by two parameters: v_b the bulk etch rate (etching rate for non-irradiated material) and v_t the track etch rate (the etching rate along the ion track). Typically the etching results in a conical or double conical pore (depending if one or both faces of the foil respectively are exposed to the etching bath) with the opening angle α: tgα = v_b/v_t [4]. In the case of high selectivity etching conditions, i.e. $v_t \gg v_b$ the shape of the pores can be approximated to a cylinder.

One can distinguish several generations of this technology. The so-colled 1st Generation used mainly polycarbonate (PC) and polyethylene terephthalate (PET) polymers that produced 10–20 μm thick microporous membranes with pores between 0.1 and 10 μm that are randomly distributed. This technology was developed in the mid-1980s by Prof. Legras and his team at UCL-POLY [29, 30]. In 1989, a first spinout, Cyclopore, was created.

Since 1996, the ion track technology has progressed considerably, due to the use of new polymers which opened up new possibilities in the control the geometry of the pores and their distribution. This technology, called 2nd Generation, makes use of polyimide (PI), which permits optimal use of the membrane up to 430 °C (PC and PET cannot be used beyond 120 °C). Apart from this, the chemical and mechanical resistance properties of PI are much better, while PI is also a well-known polymer in the field of electronics. On the other hand, PC offers several advantages: possibility to obtain easily both cylindrical or conical pores (the etching selectivity can be tuned on a wide range) and the ease to dissolve the template for direct nanostructures observation. PC dissolves easily in several organic solvents, e.g. dychlormethane. A solution containing 5 M NaOH and 10 % vol. methanol at 50 °C is typically used for producing cylindrical pores, while conical pores are obtained in an aqueous solution containing 9 M NaOH and 50 % methanol at room temperature [4, 31].

The pores of ion track membranes can be filled with metals or other polymers, obtaining therefore nanowires or nanotubes as well as other nanostructures for a broad variety of high-technology applications. The ion track templates offer a few degrees of freedom which makes them very attractive for such applications namely: (i) the possibility of preparing nanopores with the desired shape (cylindrical, conical or double conical); (ii) the possibility of choosing the desired pore density ranging from 1 pore/sample to 10^{10} pores/cm^2 by exposing the polymer foil to the desired ion fluence; (iii) the possibility of choosing the most suited material for the membrane such as polymers (polycarbonate PC, polyethileneterephtalate PET, polyimide PI), glasses, quartz or mica [32].

The method for producing membranes with pore density of 1 pore/sample was developed by the Material Research group at GSI Darmstadt. In order to obtain a single pore is necessary that the sample is hit by only one ion. Thus it is necessary to reduce the flux of heavy ions to approximately 10^3 ions/cm^2 s. A metallic plate

with thickness 0.2 mm with an aperture of 0.2 mm is inserted in front of the sample. A semiconductor detector is placed behind the sample with the purpose to detect each ion passing through the aperture and then through the sample. At such low fluxes the probability of an ion to pass through the aperture is of 1 event/s. This gives enough time to the automated system to switch of the beam using a fast chopper after an ion hit is detected by the detector.

In spite of the progress with ion track membranes, they have an essential drawback that for the preparation of ultra-small structures such as nanowires or nanotubes the first step involves the use of equipment which uses tremendous amounts of energy and has a size of at least several tens of meters namely an ion accelerator. In this sense, porous anodic aluminum oxide (AAO) membranes offer evident advantages. They attracted a remarkable interest due to the pioneer works of Martin [1] and Masuda and Fukuda [33]. Self-organized nanoporous structure with hexagonal ordered morphology were obtained on a highly pure Al surface via electrochemical anodization in acidic medium [34, 35]. Apart from the advantage mentioned above with relation to excluding the need of using an ion accelerator, AAO templates have many advantages over the polycarbonate membranes like high pore density, thermal stability, cost effectiveness and versatility. Pore diameter, length, inter-pore spacing, and pore ordering can be easily tailored by tuning the anodizing parameters such as voltage, time, electrolytes, pH value, and temperature [35].

Different acids like sulfuric acid, oxalic acid and phosphoric acids can be used for anodiziation of Al foils. Usually, sulfuric acid is used for the preparation of AAO templates with small pore diameter ranging from 3 nm to about 50 nm, phosphoric acid is used for obtaining templates with large pore diameter (≥60 nm), and oxalic acid is used to produce AAO templates with medium pore diameter. To obtain highly ordered pores, a two-step anodization was developed. For instance, in the first anodization step the Al foil is anodized at 0 °C and 40 V dc in 0.3 M oxalic acid for about 12 h to form textures on Al surface. The formed aluminum oxide layer is then removed by immersing anodized Al into a mixed solution of 0.4 M chromic acid and 0.6 M phosphoric acid solution at 60 °C. Subsequently, the sample is reanodized for different periods of time under the same anodization conditions as in the first step. Such type of self assembled AAO templates were used to fabricate different types of nanowires and nanotubes by electrochemical deposition method [36–39].

Figure 15.1 illustrates the nano-dimpled surface produced after the alumina membrane that was formed during the first anodization process was etched away. This surface serves as an ideal template for growth of an ordered structure during the second anodization in a two-step anodization process performed in potentiostatic mode at an anodization voltage of 60 V using a 0.3 M oxalic acid electrolyte [27].

Similarly to this 'nano-dimpling' seed-layer used by Sharma et al. [27] for the second anodization, Masuda et al. [40] have demonstrated a greatly improved ordering of the nanoporous structure by using a mechanical deformation pretexturing method on the aluminum foil prior to anodization.
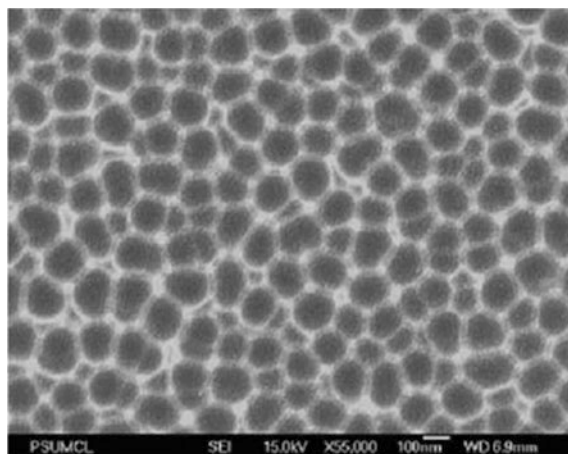
Fig. 15.1 Nano-dimpled aluminum foil after the alumina formed during the first anodization is etched away. Reprinted from Sharma et al. [27]. Copyright (2007) with permission from Springer

Figure 15.2 illustrates ordered arrays of pores with controlled diameter produced in alumina templates [41].

Alumina porous structures produced by two step anodization in a phosphoric acid solution are shown in Fig. 15.3 [42]. The first anodization step is tensiodinamic, while the second step is performed at constant voltage. The first step results in the production of the barrier-type oxide and the initiation of pores, which growth occurs during the second step by a dissolution/precipitation mechanism [43]. The residual metal is dissolved in a 0.1 M CuCl + 20 % HCl (w/w) mixture after the anodization, and the opening of the bottom side of pores is achieved by immersion in an aqueous 1 M NaOH solution at room temperature for 20 min.
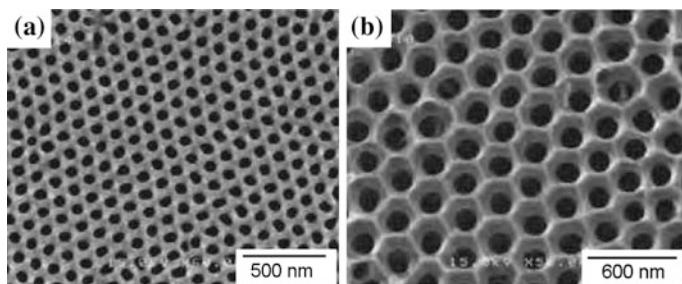

Fig. 15.2 Scanning electron micrographs of AAO templates with different pore sizes of approximately: **a** 60 nm, **b** 120 nm. Reprinted from Chen et al. [41]. Copyright (2010) with permission from American Chemical Society
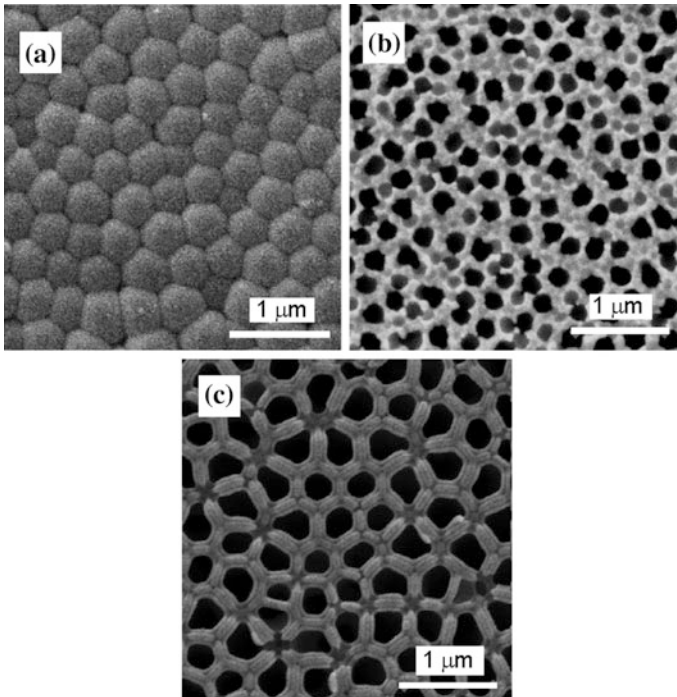
Fig. 15.3 SEM micrographs of an AAM grown in 0.4 MH$_3$PO$_4$ at 160 V and T = 10 °C after a tensiostatic charge of 160 C/cm^2: **a** metal-side surface before pore bottom opening; **b** solution side surface; **c** metal-side surface after pore bottom opening. Reprinted from Inguanta et al. [42]. Copyright (2007) with permission from Elsevier

Highly ordered alumina templates with hexagonal morphology have been also realized with a one-step anodization process in 0.4 M aqueous H$_2$SO$_4$ electrolyte at constant voltage of 26 V for 23 h using a DC power source at 0 °C [35]. Figure 15.4 shows SEM micrographs of the top and cross sectional surfaces of the produced AAO template at different magnifications. Low magnification top surface image (Fig. 15.4a) shows that the nanopores are very dense and uniform with perfect hexagonal ordering. High magnification image of the top surface (Fig. 15.4b) clearly exhibits the pore ordering and their geometry. Figure 15.4c, d shows the cross-sectional images of AAO template which reveals that the nanopores or nanochannels are very straight and parallel throughout their entire length. The authors have shown how morphology of membranes can be varied by changing anodizing parameters.

As mentioned above, both porous alumina and etched ion track membranes often play a passive role in nanofabrication due to their high resistivity. Over the last years, porous semiconductors have attracted considerable interest from the point of view of manufacturing conductive nanotemplates, especially after the demonstration of the possibility to grow self-organized [44, 45] and single crystalline
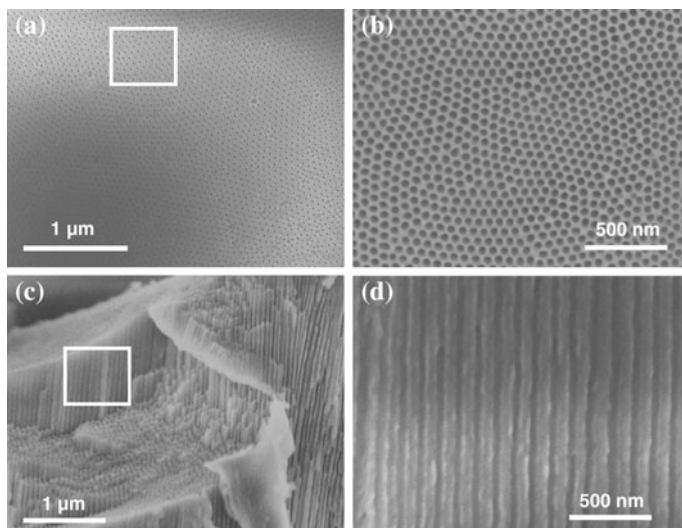
Fig. 15.4 FESEM image of AAO template. **a**, **b** Top surface view at low and high magnification. **c**, **d** Cross-sectional view at low and high magnification. Reprinted from Ali and Maqboo [35]. Copyright (2013) with permission from Springer

two-dimensional hexagonal arrays of pores by anodic etching of n-InP substrates [46–48]. The growth of arrays of parallel pores, although in a less ordered fashion, was demonstrated for CdSe as well [49]. As shown recently [50, 51], InP and CdSe nanotemplates can be produced routinely by anodic etching of crystalline substrates in salty water, the conductivity of the porous InP matrix being as high as to provide excellent conditions for the electrochemical pulsed deposition of Pt nanotubes with diameters as low as 70 nm and length up to 30 μm [51]. The electronic band gap of indium phosphide is 1.3 eV and that of cadmium selenide is 1.7 eV at 300 K, which means that the nanotemplates based on both InP and CdSe are opaque in the visible region of the spectrum. Among III–V and II–VI semiconductors one may consider the wide band gap compounds GaN (Eg = 3.3 eV), ZnO (3.3 eV) and ZnSe (2.7 eV) as good candidates for the fabrication of conductive nanotemplates transparent in the visible region. The morphology of the produced porous semiconductor templates will be shown in the Sect. 15.5.

15.3 Production of Metal Nanotubes in Ion-Track Membranes

Among the methods of filling template pores for nanofabrication are various. However, electrochemical deposition is the most direct approach and a preferred one, since a wide range of materials can be deposited this way [16, 20, 52, 53].

Electrodeposition was employed for the preparation of both metallic and semi-conductor nanowires. The first report describing a template preparation of nano-wires by electrochemical filling of pores with metals in mica dates back to more than 45 years ago [54, 55]. In contrast to electrochemical deposition which leads in most of the cases to rod-like structures, electroless deposition in nanoporous membranes can be used for the preparation of hollow structures. Therefore, it is suitable for the production of nanotubes [31, 56].

Enculescu published a review paper on nanowires and nanotubes preparation using ion track polymer membranes as templates and their characterization [4]. The first step in preparing nanowires is the deposition of a working electrode on one of the membrane surfaces by depositing a metallic thin film. In order to prepare an electrode with good adhesion to the membrane, a rough surface is preferred. For instance, sputtered deposition is performed for obtaining a gold thin film of approximately 50 nm thickness. Further, a copper layer with the thickness of about 10 μm is electrochemically deposited on top of the gold in order to completely close the pores on the electrode side and to increase the mechanical stability of the system. The sample is introduced in an electrochemical cell with the pores exposed to the deposition solution in the next step. Usually, a potentiostat in a three elec-trode arrangement is used for the deposition of the wires, and the deposition takes place in three steps. Polarization phenomena occur during the first step performed with higher current in the beginning of the process, while the actual filling of the pores with the material takes place during the second step performed with a rela-tively steady current. The third step is marked by a strong increase of the current due to the increase in deposition surface when the pores are completely filled and a cap starts to grow on the surface of the membrane. Multilayered wires can be produced by this method. For instance, the deposition of two metals in a layered arrangement can be performed from a single electrolytic bath, if the two metals are chosen in such a way that the difference between their deposition potential is high. Therefore, only the more noble metal is deposited when a lower overvoltage is applied, while an alloy of the two metals is deposited when a higher voltage is applied.

The production of nanotubes by electroless deposition in ion track membrane is based on the feature of the process that the deposition takes place only on the catalytic surface. Therefore, the pore walls can be covered with the desired material avoiding completely filling. As compared to the electroless deposition on macro-scopic surfaces, in order to achieve complete tubes, it is necessary to give time to the reactants to reach all over the pore, i.e. the reduction reaction should be slow in order to compensate for the diffusion. To create a large number of catalytic nuclei on the surface, a three step process is employed with a preactivation (for instance with Sn^{2+} ions), and an activation deposition (for instance with Pd) [4]. Such a three step process was applied by Enculescu et al. [32] for the preparation of nano and microtubes of nickel in polycarbonate ion track membranes using the electroless deposition from an acidic bath containing nickel chloride as a source of nickel ions, nickel citrate, sodium hypophosphite and sodium acetate. It was mentioned that the preactivation process is the most important one during the entire deposition, and

this process should be carefully controlled. It was also observed that the deposition takes place in very good conditions when the polymer surface which typically is hydrophobic becomes hydrophilic. The activation occurs during the second step when the template membranes is dipped in a solution containing Pd^{2+} ions and the following reaction takes place: $Sn^{2+} + Pd^{2+} \rightarrow Sn^{4+} + Pd^0$. Palladium colloids are formed on the surface of the samples as a result of this reaction, which constitute the catalyst for the deposition reaction. In commercial electroless metal deposition, a more stable and easier reproducible 2 step process is preferred, which consists in the activation with palladium colloids stabilized by Sn^{4+} ions and afterwards the deposition process.

However, the 3 steps process presents a major advantage for the preparation of very small objects, since the number of Pd nuclei which can be obtained on the surface is one order of magnitude higher than in the 2 steps procedure. This allows the deposition of thinner metal films with higher adhesion to the surface.

The process of metal deposition (for instance Ni) is mainly associated with the reduction of metal ions from the solution in the presence of the catalyst. The main chemical reactions which take place in the deposition process are, for instance:

- the oxidation of the hypophosphite ions in the presence of catalytic surfaces into ortophosphite ions;
- the reduction of metal (Ni) ions.

During the deposition process in the presence of catalytic surface the hypophosphite ions oxidize in ortophosphite ions. The hydrogen atoms which result in this reaction are partially adsorbed onto the catalytic activated surface, where the metal (Ni) reduction reaction takes place, metallic nickel being deposited onto the surface.

In spite of the fact that the electrodeposition process of metal only along the pore walls is not sufficiently controlled relative to an electroless plating method, Motoyama et al. demonstrated that both metal nanowires and nanotubes can be produced by controlling the initial stages of electrochemical growth in PC membranes by using a sputter-deposited Pt–Pd layer as the cathode, which was so thin that the pores at the bottom were opened to pathways for the electrolyte [28]. The growth of Cu nanowires was deduced from the abrupt decrease in the cathodic current during the Cu deposition, which was correlated with the progress of the Cu grain growth and plugging the pores with the coarse Cu grains on the Pt–Pd side. In contrast to this, both nanowires and nanotubes were obtained with electrodeposition of Ni. The observed abrupt decrease in the cathodic current was associated with a nanostructure transition from the tube to the wire occurring at the growth front in this case. The authors mentioned that the important combination of the nanoporous template with a size distribution of metal grains must be emphasized when the nanostructured interface is designed. It was observed that the growth rate of the Ni tubes along the length was one order faster than that for the wall thickening. Therefore, it was found that the Ni nanotube growth lasts for longer deposition times as compared to Cu nanotube, which growth is lost immediately after the beginning of the electrodeposition.
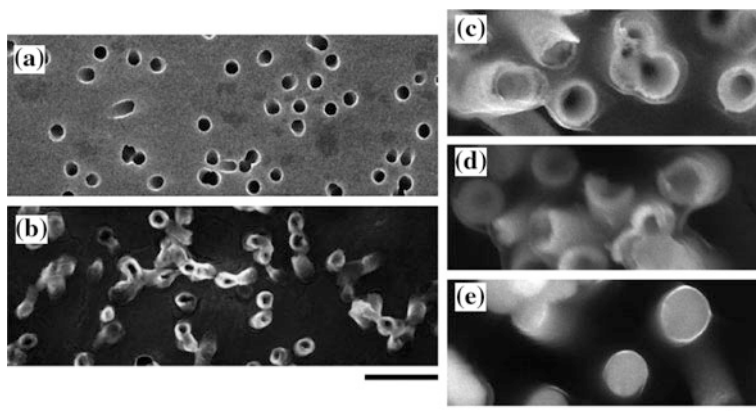
Fig. 15.5 SEM images of the sputter-deposited Pt–Pd layer on the PC membrane template with the pores of 200 nm in diameter (**a**, **b**), and of nanostructures formed at different deposition times (**c**–**e**). *Scale bar* 1.0 μm (**a**, **b**); 200 nm (**c**–**e**). The sputtered side (**a**). The Pt–Pd nanotubes liberated from the PC membrane (**b**). The deposition time for Ni nanostructures is 7 s (**c**); 15 s (**d**); 32 s (**e**). Reprinted from Motoyama et al. [28]. Copyright (2007) with permission from Elsevier

Figure 15.5a shows the Pt–Pd surface on the template membrane with the pores of 200 nm in diameter. It is clearly seen that the pores are not sealed and the original diameter is maintained. The image of the liberated Pt–Pd tubes as the cathode after the dissolution of the membrane with a dichloromethane solution is shown in Fig. 9.5b. The height of the nanotubes is roughly 300–500 nm. The growth of Ni nanostructures into the PC membranes is illustrated in Fig. 15.5c–e after the template membrane was dissolved in dichloromethane. Hollow tubes with wall thicknesses of 20–40 nm are produced at the deposition time of 7 s (Fig. 15.5c), which demonstrates that deposition of nickel occurs only along the pore walls from the edge of the Pt–Pd tubes as the cathode. The Ni tube walls become thicker gradually to reach a thickness of roughly 50 nm at the deposition time of 15 s (Fig. 15.5d). Finally, the top surface no longer shows a hollow cross-section at the deposition time of 32 s (Fig. 15.5e), i.e. nanowires are produced instead of nanotubes.

15.4 Metal Nanotubes in Porous Alumina Templates

Electrochemical deposition is also widely used for the nanofabrication in porous alumina templates. Basically, three kinds of electrochemical deposition methods are applied for filling the pores of AAO template: direct current (DC) electrodeposition [57], pulse electrodeposition (PED) [24], and alternating current (AC) electrodeposition [58].

The preparation of the AAO template for filling with metallic or magnetic materials via DC electrodeposition consists of several steps such as dissolving the

Al substrate in a saturated solution of HgCl$_2$, etched away of the barrier layer using chemical etching, sputtering of a thin metallic contact on one side of AAO which act as a cathode during electrodeposition. Etching away of the barrier layer often leads to the non-uniform widening of pores at the bottom and production of AAO template with different pore diameters at the top and the bottom surface, which ultimately results in non-uniform-diameter nanostructures. Additionally, these steps are time consuming, and the DC electrodeposition in porous AAO without modification of barrier layer is generally unstable and leads to a non-uniform filling of the AAO nanopores due to the cathodic side reaction [24, 35]. The uniformity and
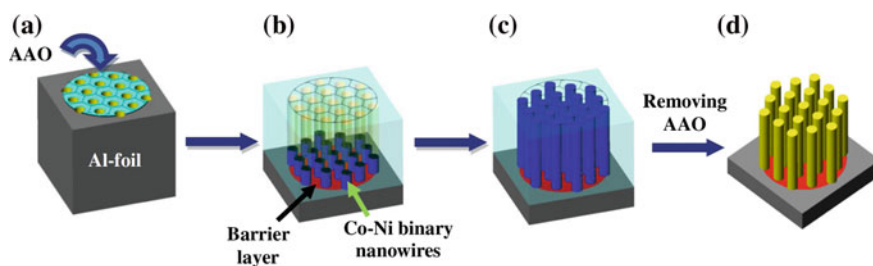

Fig. 15.6 Schematic diagram for co-deposition process of Co-Ni binary nanowires in nanopores of AAO template. **a** AAO template with *circular* shape, **b** filling of nanopores started from Co-Ni binary nanowires at the *bottom* of AAO by exposing circular area to the Co and Ni precursor solution, **c** complete filling of the alumina nanopores from Co-Ni binary nanowires, **d** dissolution of alumina in NaOH to get Co-Ni binary nanowires. Reprinted from Ali and Maqboo [35]. Copyright (2013) with permission from Springer
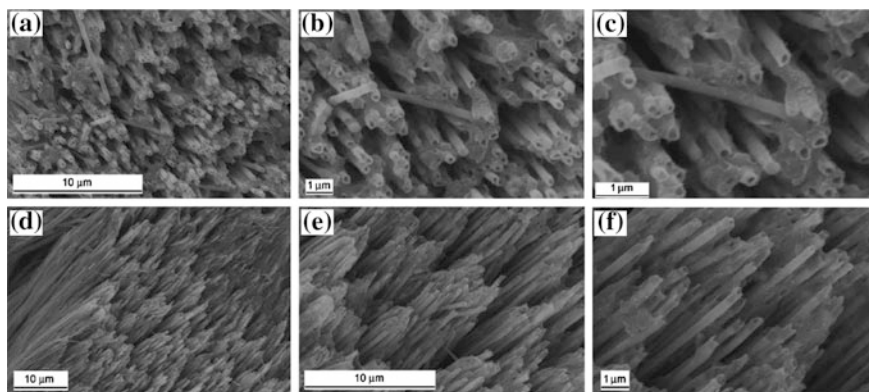

Fig. 15.7 SEM images of iron nanotube arrays: **a** *top view*, magnifying power K5000; **b** *top view*, magnifying power K10000; **c** *top view*, magnifying power K20000; **d** *side view*, magnifying power K2000; **e** *side view*, magnifying power K5000; **f** *side view*, magnifying power K10000. Reprinted from Cao et al. [59]. Copyright (2006) with permission from John Wiley and Sons

pore-filling efficiency increased many folds when the PED method is used compared to DC electrodeposition. However, PED method also needs modification of the barrier layer [24]. In contrast to this, AC electrodeposition is simpler in the sense that it does not need the detachment of AAO template from the Al substrate or modification of the barrier layer. Moreover, since the Al-substrate is not removed, it can be used as cathode during electrodeposition. The AC deposition of Co-Ni binary alloy nanowires without modifying the barrier layer at room temperature was reported by Ali et al. [35]. A schematic diagram of the used metallic deposition is shown in Fig. 15.6.

Cao et al. reported a systematic preparation of well-aligned metal (Fe, Co, Ni) nanotubes into pores of the alumina template and proposed their growth mechanisms. The production of Fe nanotubes is illustrated in Fig. 15.7.
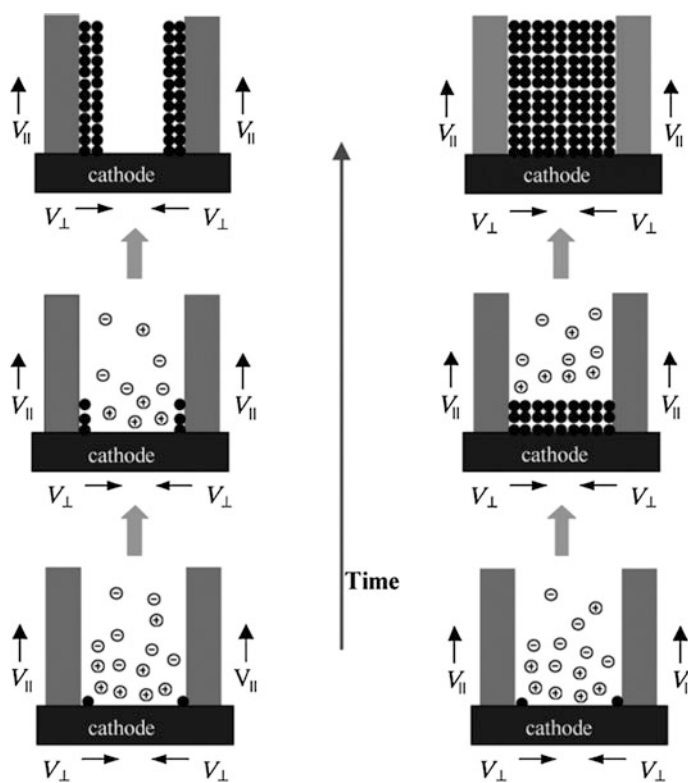
Fig. 15.8 Schematic diagram of the growth mechanism of 1D metal nanostructures via the template-based electrochemical deposition method. **a** Metal nanotube growth steps. **b** Metal nanowire growth steps. Reprinted from Cao et al. [59]. Copyright (2006) with permission from John Wiley and Sons

The schematic diagram of the electrodeposition process proposed by Cao et al. [59] is presented in Fig. 15.8. According to this diagram, the metal ions, surrounded by a hydration layer, move toward the cathode, where they are reduced. The reduction process consists of three steps: (i) the hydration number of metal ions decreases and the metal ions are rearranged in solution near the cathode surface; (ii) metal ions surrounded with partly discarding water molecules are reduced; (iii) adsorbed metal atoms discard the surplus hydration layer, then enter the crystal lattice. According to this growth mechanism of metal nanotubes, the junction between the cathode surface and the bottom edge of the template pore serves as a preferential site for the deposition of metal ions.

Similarly to processes occurring during the preparation of porous membrames, where the shape and size of the pore are determined by the ratio of two parameters: v_b and v_t as described above, the morphology of nanostructures produced into porous alumina template (i.e. nanowires or nanotubes) is determined by two parameters: $v_{\parallel}$ (growth rate parallel to current direction) and $v_{\perp}$ (growth rate perpendicular to current direction). At low current density, these rates are nearly equal each other ($v_{\parallel} \approx v_{\perp}$) and metal atoms fill most of the template pores until the pores are completely filled, wirelike 1D nanostructures being obtained. At high current density, the growth direction parallel to the current direction is the preferential one, which means that $v_{\parallel} \gg v_{\perp}$, and tubular structures are generated.

A similar mechanism was proposed for the growth of Pt nanotubes [60]. Pt nanowires, thick-wall nanotubes and hollow (or thin-wall) nanotubes have been prepared by DC deposition in AAO templates (Fig. 15.9). Nanowires and hollow nanotubes are clearly observed in Fig. 15.9b with a considerable contrast difference, while thick-wall nanotubes can be observed in the middle of Fig. 15.15c. Some of the images showed ruptured parts on nanotubes (left-hand nanotube in Fig. 15.9d). The SEM images of Pt nanowires and nanotubes shown in Fig. 15.9 are well explained according to the above described model (Fig. 15.10a), i.e. nanowires are produced with low-current condition, when Pt metal is relatively slowly electroplated, while nanotubes are obtained with high-current condition, when metal plating starts to generate a tube-like structure from the plasma-sputtered Au on the bottom surface of the AAO membrane and a portion of the inside channel surface. By making use of this model, the authors were able to prepare novel core-shell cable structure of metal alloys (Fig. 15.10b) by stopping the growth of nanotubes of one metal in a high-current-density condition before the surface AAO channels became clogged and subsequently electroplating a second metal within the generated nanotubes at allow current density to fill up the nanotubes.

The growth of metal nanotubes along the pore walls of an AAO membrane by means of of metallic nanoparticles immobilized on the wall surfaces has been also
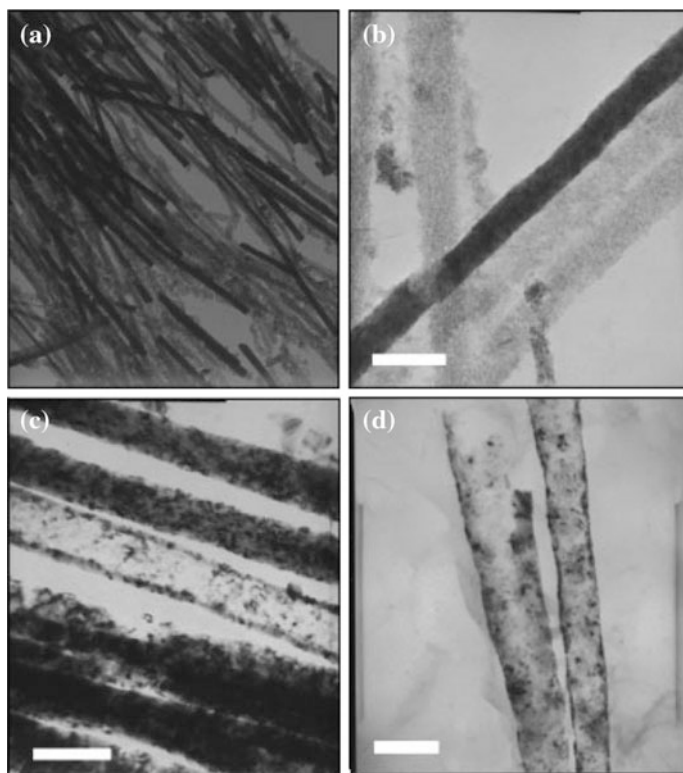
Fig. 15.9 Pt nanowires obtained by the high-current-density plating method. **a** TEM image at low magnification, **b–d** three different kinds of Pt nanostructures (close-packed nanowire, thick-wall nanotube, and hollow nanotube) (*scale bar* is 100 nm). Reprinted from You and Lee [60]. Copyright (2004) with permission from John Wiley and Sons

performed by Lee et al. [61] (Fig. 15.11). Particularly, Ag nanoparticles have been immobilized on the pore walls, followed by the production of Au nanotubes. As described above, the growth of metal nanotubes in this process starts at the base-metal electrode at the bottom of the pores as a result of the nonconducting nature of the nanochannels. The nanotube formation in this electrodeposition process was explained in terms of the relative rates of deposition and the diffusion of metal ions by assuming that the deposition process takes place at the tube tips, and therefore the deposition interfaces and the diffusion layers of metal ions move dynamically with the growth process of the tubes as shown in Fig. 15.11. The conducting path is created by electrodeposition between the tube tip and an isolated Ag nanoparticle, and the deposition interface moves from one isolated nanoparticle to another one via the dynamically created conducting paths.
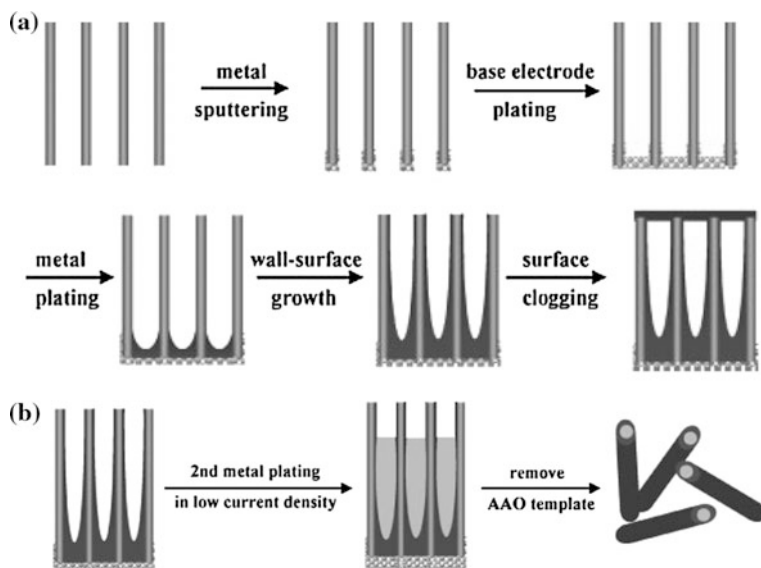
Fig. 15.10 **a** Postulated growth pattern of metal nanostructures by electroplating. **b** Preparation of core-shell nanocable metal alloys by consecutive electroplating at different current densities. Reprinted from You and Lee [60]. Copyright (2004) with permission from John Wiley and Sons

This method results in the production of mixed-metal nanotubes (i.e. Au nanotubes with surfaces decorated with Ag nanoparticles) upon the removal of the oxide matrix. The authors used this method for the preparation of multisegmented metallic nanotubes with a bimetallic stacking configuration along the nanotube axes as shown in Fig. 15.12. It was shown that the design of such multisegmented metallic nanotubes, i.e. the length of each metal segment, can be tuned by controlling the amount of total integrated charges involved in the electrochemical reaction, and such tailoring of the nanotube structure provides fascinating opportunities for engineering the physical properties of nanotube materials.

Apart from electrochemical deposition, electroless deposition can also be employed for the preparation of metal nanotubes into porous alumina templates. Inguata et al. performed nickel electroless deposition from a bath containing Ni sulfate as nickel source and sodium hypophosphite as reducing agent in order to fabricate Ni nanotubes [42]. The surface of pores was sensitized/activated by dipping the membrane alternatively (10 times) in a sensitization solution, containing $SnCl_2$, and in an activation solution containing a Pd salt. The Ni electroless deposition was also performed in five steps, each lasting 4 min, by adding to the same bath the overall quantity of the reducing agent (1.4 g/L). The entire membrane
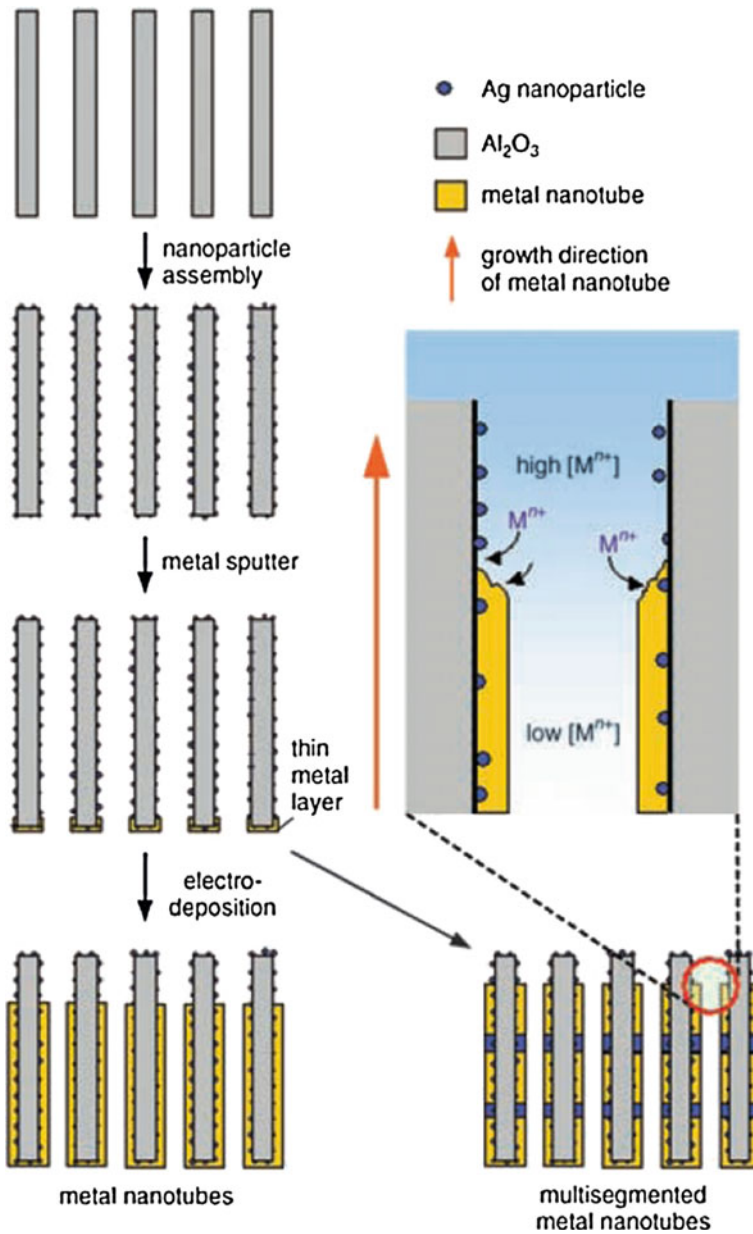
Fig. 15.11 Procedure for the preparation of metal nanotubes and the proposed mechanism of metal nanotube growth (see text). Reprinted from Lee et al. [61]. Copyright (2005) with permission from John Wiley and Sons
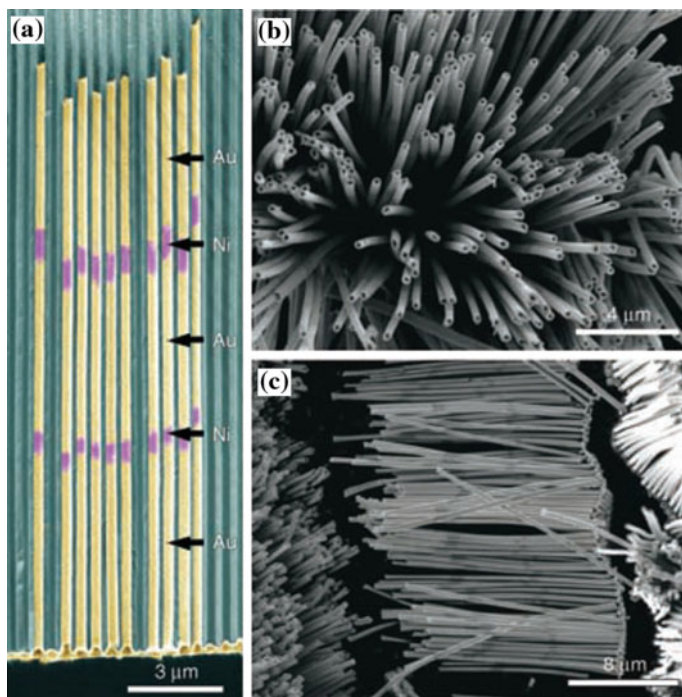
Fig. 15.12 SEM images of multisegmented metal nanotubes with a stacking configuration of Au-Ni-Au-Ni-Au along the nanotube axis. **a** Cross-sectional SEM image of as-prepared metal nanotube–AAO composite, which shows metal nanotubes embedded in an alumina matrix. The signals from Au and Ni are shown in *yellow* and *purple*, respectively. **b**, **c** SEM images of multisegmented metal nanotubes after removal of alumina matrix; part **c** clearly shows the stacking configuration of multisegmented metal nanotubes in which the segments with *bright* and *dark* image contrasts correspond to Au and Ni, respectively. Reprinted from Lee et al. [61]. Copyright (2005) with permission from John Wiley and Sons

surface was covered by Ni spherical grains forming a continuous and dense metal layer after 5 deposition steps as illustrated in Fig. 15.13.

Sung et al. [62] proposed an alternative to electroless and electrochemical deposition method for the production of metal nanotubes in porous alumina templates termed as "two step evaporation method". The method is based on evaporation processes to inject aluminum vapors into the porous template. The aluminum is deposited on the surface of the porous template by vacuum evaporation in the first step, and the deposited aluminum is vaporized and forced to be injected into pores by heating the sample at atmospheric pressure during the second step.
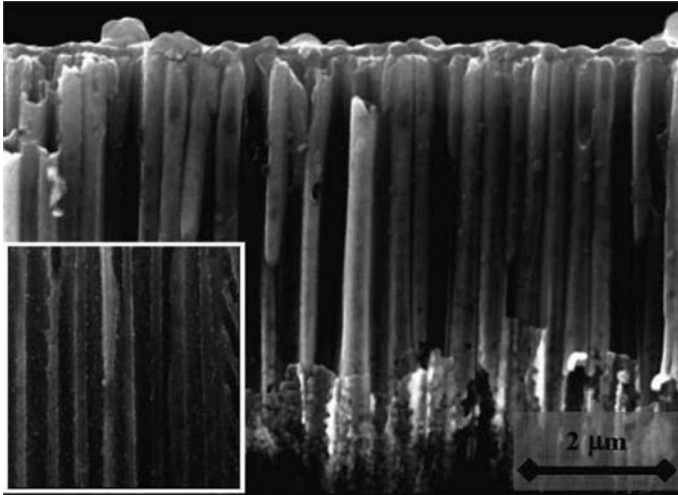
Fig. 15.13 SEM micrograph of the upper part of pores for a commercial AAM after 5 electroless deposition steps. *Inset* is the central part of the channel. Reprinted from Inguanta et al. [42]. Copyright (2007) with permission from Elsevier

15.5 Semiconductor-Metal Nanocomposites on the Basis of Metal Nanotubes Deposited in Semiconductor Templates

As mentioned in the Sect. 15.2, conducting nanotemplates for nanofabrication are produced on semiconductor substrates by anodic etching. The first III–V semi-conductor templates, including those with self-organized two-dimensional hexag-onal arrays of pores have been prepared on InP substrates. Crystalline (100)-oriented substrates of sulfur doped n-InP with 500 µm thickness and free electron concentration of 1.3×10^{18} cm^{-3} were used for these purposes [51]. Anodic etching was carried out in dark at room temperature in NaCl aqueous solution. It was shown that the diameter of the produced pores is controlled by the concentration of the used electrolyte, pores with diameters of about 70 or 140 nm being obtained with 3.5 or 1.7 M NaCl aqueous solutions, respectively. Figure 15.14a presents a cleavage of a porous sample produced by anodic etching of n-InP substrate in 1.7 M NaCl aqueous solution for 1.5 min, with subsequent removal of the nucleation layer. Anodization of n-InP in aqueous solution of NaCl proves to be an effective approach for the purpose of uniform nanostructuring and fabrication of semicon-ductor nanotemplates with ordered distribution of pores. These pores are oriented along current lines and they show usually circular shape, independent upon the crystallographic orientation of the substrate. A fascinating property of the current line oriented (CLO) pores is their long-range interaction in the process of formation, leading under certain conditions to self-arrangement in 2D hexagonal close packed

lattice. The CLO pores with transverse dimensions of about 140 nm distributed in 2D hexagonal arrays are clearly seen in Fig. 15.14a.

Nanotubes have been produced into these templates by electroctrochemical pulsed deposition of Pt with the duration of cathodic pulse of 300 μs for Pt deposition in pores with diameters 140 nm, which leads to uniform metal deposition on inner surface of pores (Fig. 15.14b).

Porous ZnSe templates present even more interest, since they are transparent for the visible light due to their larger bandgap. A method has been developed for controlling the conductivity of ZnSe crystals [63], which in its turn determines the diameter of the produced by anodization pores. It is based on doping the samples with Al from a Zn + Al melt. Figure 15.15a illustrates the production of a porous template on 1 mm thick n-ZnSe substrate with free electron concentration of 7×10^{16} cm^{-3}. The anodic etching was carried out in dark at room temperature in a $K_2Cr_2O_7$:H_2SO_4:H_2O electrolyte with the ratio 5:100:10 [64]. Although the formation of uniformly distributed pores exhibiting features of short-range order is
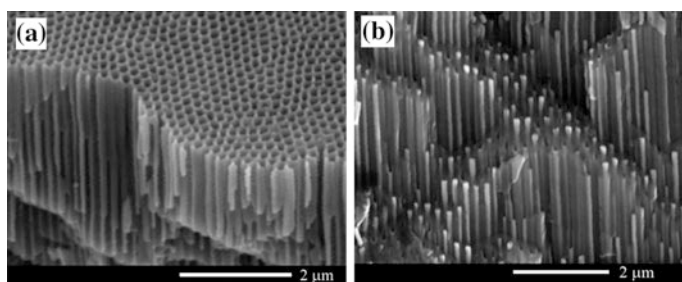

Fig. 15.14 SEM images taken from n-InP template prepared on (100)-oriented substrate with free electron concentration of 1.3×10^{18} cm^{-3} by anodization in 1.7 M NaCl aqueous solution (**a**); and SEM image taken from a cleaved porous template after pulsed electrodeposition of Pt (**b**)
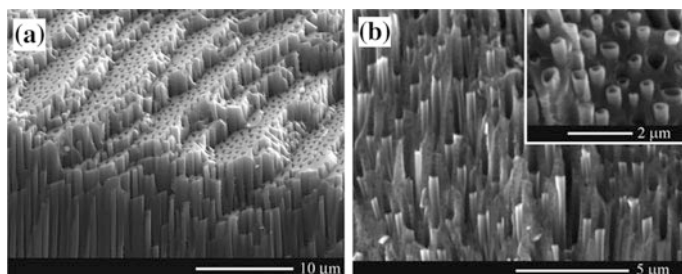
Fig. 15.15 SEM images taken from n-ZnSe template prepared by anodization in a $K_2Cr_2O_7$: H_2SO_4:H_2O electrolyte with the ratio of 5:100:10 (**a**); and SEM image taken from a cleaved template after pulsed electrodeposition of Pt (**b**). The *insert* in (**b**) illustrates a *top view* after the sample was additionally cleaved along a plane nearly perpendicular to the pores

inherent to anodic etching of n-ZnSe, long-range order in pore distribution was not reached. The reason could be the absence of crystallographically oriented pores in ZnSe. It is well known that the long-range order in pore distribution evidenced in n-InP is favored by the network of crystallographically oriented pores initially formed in the nucleation layer [46]. In case this network is well developed, there is a general tendency of current-line oriented pores to form rows oriented along $\langle 110 \rangle$ direction.

Pt electroplating in pulsed voltage regime in 20 μm thick porous ZnSe layer with diameters of pores of about 400 nm was carried out at 40 °C for 8 h in a common two-electrode plating cell containing 2 g/l Pt where the porous sample served as working electrode, while a platinum wire was used as counter electrode. During the 200 μs pulse time a cathodic potential of −40 V was applied between the two electrodes to electrochemically reduce the metal species on the inner surface of the porous matrix in contact with the electrolyte. After each pulse a delay time as long as 1 s was used at zero external voltage applied to allow ions to diffuse into pore regions depleted during the deposition pulse. Besides, magnetic stirring was applied to provide recovery of the ion concentration in the electrolyte along the whole depth of pores. As one can see from Fig. 15.15b, electrochemical deposition of Pt resulted in the formation of metal nanotubes with the wall thickness of about 50 nm. Pieces of Pt nanotubes getting out from pores are clearly seen in the cross-sectional view taken from a cleaved sample, see insert in Fig. 15.15b. The quality of nanotubes is indicative of good uniformity of metal deposition on the inner surface of pores.

The possibility to fabricate two-dimensional metallo-semiconductor quasi-periodic structures has been also demonstrated with porous GaP templates [65]. Templates with parallel pores possessing diameters in the micrometer and sub-micrometer ranges have been fabricated by electrochemical etching of commercially available n-GaP substrates with (100) orientations and electron concentration of about 10^{17} cm^{-3} in H_2SO_4 aqueous electrolyte.

Figure 15.16a illustrates the morphology of a porous GaP template. Similarly to InP templates, ordered arrays of pores are produced due to self-organization phenomena occurring during the pore growth. The white lines in Fig. 15.16a mark several directions of pore alignment in a porous GaP template. Uniform electroplating of Pt on inner surface of pores was realized in acid platinum bath under pulsed voltage regime, the deposition being performed at 40 °C in a common two-electrode cell where the porous sample served as working electrode and a platinum wire was used as counter electrode. It was found that under pulsed voltage regime it is possible to deposit metal within limited regions in depth of the porous structures, the depth of these regions being mainly dependent upon the ratio between the pulse duration and delay time between pulses. Electroplating starts with the deposition of metal dots, their density increasing with time. Overlapping of neighboring dots leads to the formation of tubular structures, as illustrated in Fig. 15.16b. It was found that the application of short pulses (<0.3 ms) during electroplating results in a predominant deposition of Pt near the bottom of the pores, while longer pulses lead to the predominant deposition near the mouth of the pores. So, the pulse length of 0.3 ms was found to be optimal for a uniform metal
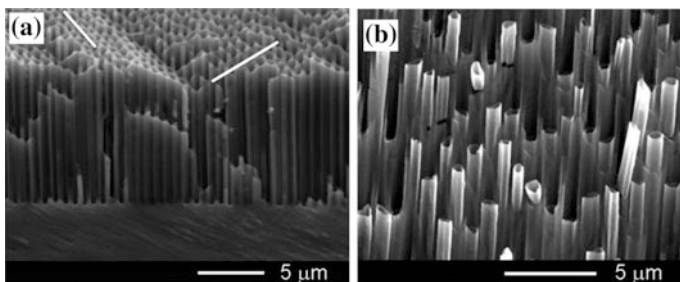
Fig. 15.16 SEM image of a porous GaP template with ordered arrays of pores indicated by *white lines* (**a**) and an image illustrating the formation of Pt cylindrical tubular structures (**b**)

deposition inside the pores of the template, metal tubes with smooth walls with rather good mechanical strength being produced.

Since the GaP template is characterized by ordered arrays of pores, it was found that packs of rows of Pt nanotubes in semiconductor envelope can be easily cleaved from the sample. Actually the semiconductor nanotemplate with the embedded array of metal nanotubes behaves like a layered crystal, the role of individual layers being played by the rows of Pt nanotubes in n-GaP envelopes. The possibility of such a cleavage is important from the point of view of photonic applications of the produces metallized porous GaP templates as discussed in the next section of the paper.

15.6 Applications

As mentioned in the introduction section of this paper, nanomaterials based on porous nanotemplates find wide applications in electronics, optics, computers and communications, magnetism or biomedical sciences. For instance, a device with the metal deposited in a porous semiconductor template can find applications in solid-state electronics, since a system of two interpenetrating networks is formed that has a very large interfacial area [66]. The huge surface of a Schottky contact implies an enormous capacitance, which has been exploited in a variable capacitance device developed on two-dimensional metallo-semiconductor networks prepared by pulsed electrochemical deposition of Pt inside porous GaP membranes with parallel pores possessing diameters in the micrometer and sub-micrometer ranges [65]. The morphology of Pt nanotubes deposited into porous GaP template used for the fabrication of such a device is shown in Fig. 15.17a. As concerns the characteristic sizes of a template for a capacitance semiconductor device, i.e. the pore diameter and the thickness of the skeleton walls, they should be chosen taking into account the value of the depletion region. The operation of the device to be realized is based on the overlapping of the depletion regions in the skeleton walls, starting from a certain applied bias. The rapid change of the device capacitance starts from this voltage and takes place up to the voltage of overlapping the
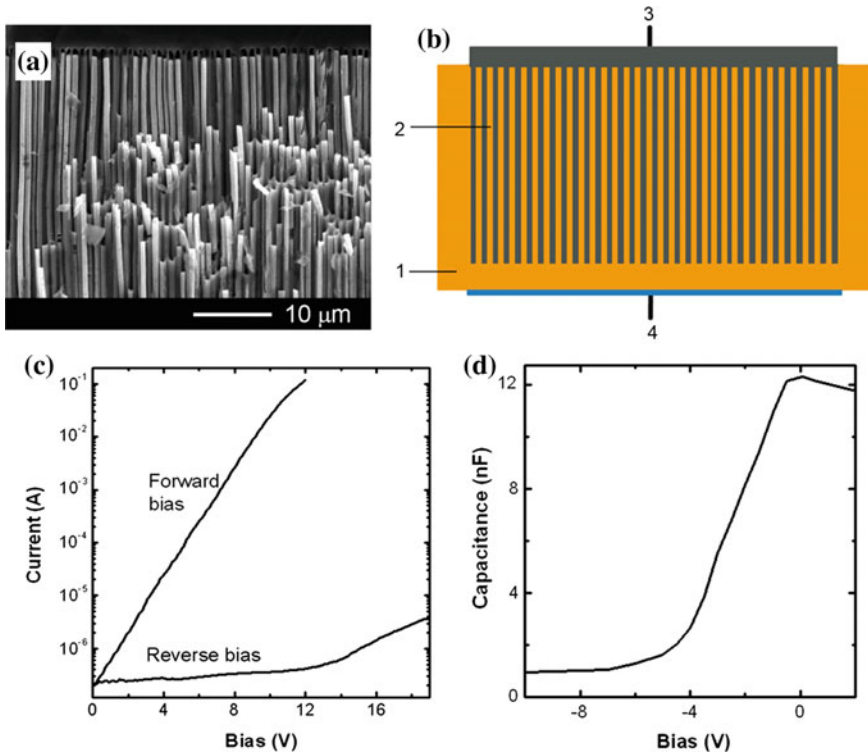
Fig. 15.17 **a** The morphology of Pt nanotubes/porous GaP nanocomposite used for the fabrication of a variable capacitance device. **b** The schematics of the device: *1* GaP substrate; *2* porous GaP template with Pt nanotubes; *3* Pt Schottky contacts deposited inside the pores and on the frontal surface of the template; *4* Ohmic contact. **c** Current-voltage characteristics. **d** Capacitance-voltage characteristics

depletion regions in the whole semiconductor skeleton. Therefore, the width of the walls cannot be less than the double depletion region at zero applied voltage for a given material. The real value of the barrier height in a Pt-*n*-GaP Schottky contact is about 1.1–1.3 eV. One can deduce a width of the depletion region of about 70–80 nm at zero applied voltage in a *n*-GaP specimen with free electron concentration of 10^{17} cm^{-3}. Therefore, the width of the skeleton walls cannot be smaller than 150 nm. The produced templates satisfy these conditions. Figure 15.17b presents the schematics of the device. The GaP porous layer was produced in the depth of 70 μm in a 500-μm thick substrate through an open window with the surface of 0.5 mm^2 on the front side of the GaP wafer. The Schottky contact was formed on the top and inner surfaces of the template, while the ohmic contact was formed on the back side of the substrate through the deposition of In. The current-voltage characteristics of the produced device structure are shown in Fig. 15.17c. The device shows a rectification ratio around 10^5 at the bias of 12 V.

The dependence of the device capacitance upon voltage is presented in Fig. 15.17d. One can see from this characteristic that the capacitance demonstrates a sharp decrease from 12 to 2 nF when the reverse bias is changed from 0.5 to 4 V, it means that the device demonstrates a capacitance density variation as high as 6×10^{-3} picofarad per square micron per volt. This value is much higher than that inherent to a variable capacitance device formed by the diffusion of dopants into a semiconductor material to form a flat p-n junction, or by the deposition of a metal that forms a Schottky contact with a flat semiconductor.

From the point of view of photonic applications, one-dimensional metallo-dielectric multilayer structures prove to be transparent in specific spectral regions and exhibit negative refraction and subwavelength imaging [67, 68]. Two-dimensional metallo-dielectric structures, to which the nanotubes deposited into porous templates belong, are even more prospective for photonic applications, for instance, for the development optical elements based on negative index materials (NIMs). NIMs with $n_{eff} = -1$ ($\varepsilon_{eff} = -1$; $\mu_{eff} = -1$) provide the opportunity for building a "perfect lens" that can focus electromagnetic waves to a spot size much smaller than the wavelength of the radiation [69, 70].

The importance of semiconductor nanotemplates with metal nanotubes grown inside the pores for photonic applications was demonstrated by calculations of some photonic properties. A highly efficient and accurate multiple-scattering approach is usually used to calculate the propagation of electromagnetic waves through the designed structures [71].

In order to investigate the photonic properties of materials assembled from porous templates with metallized pores, a simplified method was used which is based on the analysis of a parameter f describing the difference from the point of view of light scattering properties between the investigated material and a similar one with identical geometrical parameters but assembled from rods with the refractive index n = −1:

$$f = \max \left| D_m^{ni} - D_m \right|_{10 > m > -10}$$

where D_m^{ni} and D_m are the parameters determining the light scattering properties of the material assembled from rods with n = −1 and the investigated material, respectively; m is the index of the cylindrical function [71, 72].

The results of calculation of the parameter f for a metallized porous GaP template with close packing of pores, i.e. for the diameter of pores equal to the lattice parameter are shown in Fig. 15.18a. Ag was used for metallization since its plasma frequency lies in the near UV spectral range. The optical properties of Ag used in calculations were assumed to be described by the Drude formula with the plasma frequency $\omega_p = 4$ eV and damping parameter $\gamma = 0.01$ eV.

The focusing properties of flat lenses designed from porous GaP templates were studied by calculating the transmitted through the lens electromagnetic power $T = (E/E_0)^2$, where E is the electric field amplitude of the radiation passed through the lens, and E_0 is the electric field amplitude without the lens. In Fig. 15.18b, each
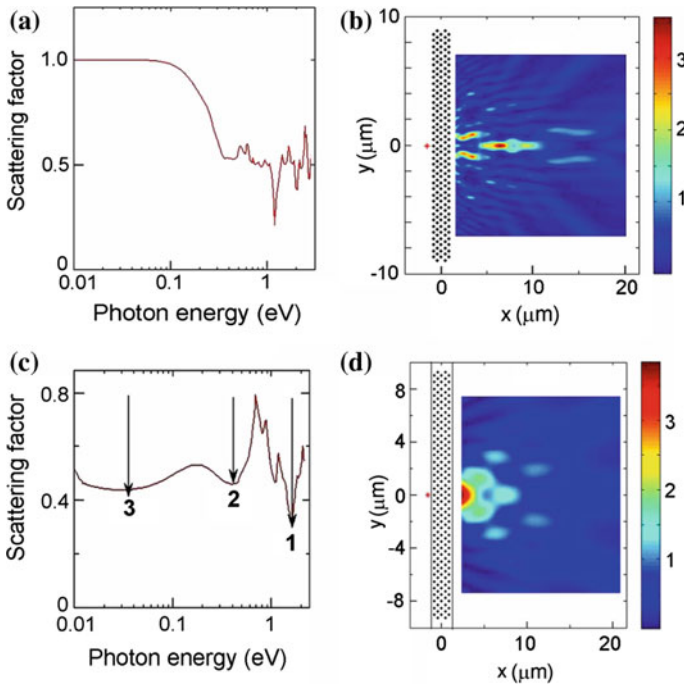
Fig. 15.18 **a** Spectral dependency of the parameter *f* for a porous GaP template with the diameter of pores 500 nm covered by an Ag film with thickness of 44 nm arranged in a *triangular* lattice with the lattice parameter of 500 nm. **b** Focusing properties of a flat lens designed from a porous GaP template as described in (**a**) calculated for the wavelength corresponding to the minimum in the spectral dependency of the *f*-parameter. **c** Spectral dependency of the parameter *f* for a porous GaP template with the diameter of pores 500 nm covered by a metallic film with the thickness of 100 nm and the refractive index n = 100 +200i, arranged in a *triangular* lattice with the lattice parameter of 500 nm; **d** focusing properties of a flat lens designed from a porous GaP template, as described in (**c**), and calculated for the wavelengths corresponding to the minima 2 in the spectral dependency of the *f*-parameter

black point from the flat lens represents a metallized pore, its axis being oriented perpendicularly to the plane of the figure. One can see from Fig. 15.18b that the focusing properties of such a lens are very good.

When investigating the photonic properties of the designed structures at longer wavelengths, one should take into consideration that the dielectric constant of the metal is not appropriately described by the Drude model al long wavelengths where it is characterized by high values of the real and imaginary parts. Having this in mind, calculations have been performed for porous GaP templates with pores covered by a metal with the refractive index n = 100 +200i which is realistic for some metals at low frequencies. As one can see from Fig. 15.18d, this kind of photonic lenses demonstrates also good focusing properties in the infrared spectral range.

Operation of photonic crystal lenses at infrared wavelengths has also been demonstrated on the basis of InP based photonic crystal technological platform including hole and pillar networks fabrication at nanometer scale [73]. Moreover, a two-dimensional device mixing arrays of holes and pillars was evaluated to pave the way for future integrated nanophotonic devices with complex functionalities such as cloaking or routing functions at optical wavelengths [74], detection and/or imaging [75].

It was shown that metallized titania nanotubes are also promising for designing and manufacturing negative index materials [72]. Flat and concave lenses assembled from these nanotubes demonstrate good focusing properties at specific photon energies which are determined by the geometry of nanotubes and features of their spatial distribution. The parameters of the produced TiO_2 nanotubes can be controlled by adjusting the technological conditions of anodizing Ti foils. Particularly, it was shown that the anodization of Ti sheets in an ethylene glycol and HF containing electrolyte allows one to prepare TiO_2 nanotubes with the inner diameter controlled in the range from 10 nm to more than 250 nm through the change of the electrolyte temperature from −20 to +50 °C [76]. Figure 15.19 illustrates the morphology of TiO_2 nanotubes produced at the electrolyte temperature of 0 and +30 °C.

The results of calculation of focusing properties of a concave lens assembled from titania nanotubes (n = 2.6) with the inner diameter of 80 nm and the outer diameter of 160 nm the outer and inner surfaces being covered with an Ag film with thickness of 12 nm are shown in Fig. 15.20.

The focusing properties of flat lenses assembled from metallized titania nanotubes proved to be not so good as those of concave lenses (Fig. 15.21a). However, it was found that these properties can be improved by assembling the flat lens from a superlattice of optimized clusters instead of ordered nanotubes (Fig. 15.21b). A clear superlensing effect is observed with the superlattice of optimized clusters i.e. $S/\lambda^2 < 1$, where S is the surface of the focal spot.
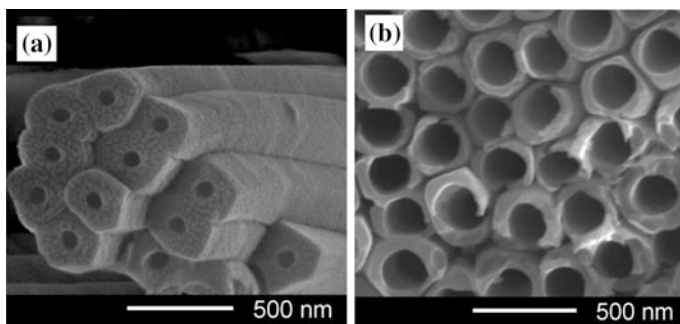

Fig. 15.19 SEM images of TiO_2 NTs prepared by anodization of Ti sheets at the electrolyte temperature of 0 °C (**a**) and +30 °C (**b**)
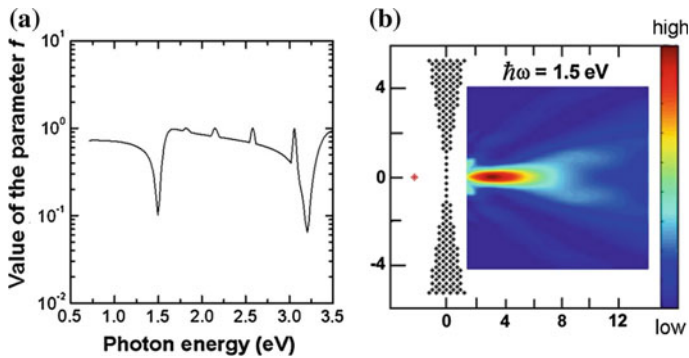
Fig. 15.20 The spectral dependence of the parameter f for titania nanotubes with the inner diameter of 80 nm and the outer diameter of 160 nm metallized by an Ag film with thickness of 12 nm (**a**), and focusing properties of a concave flat lens designed from these nanotubes (**b**)
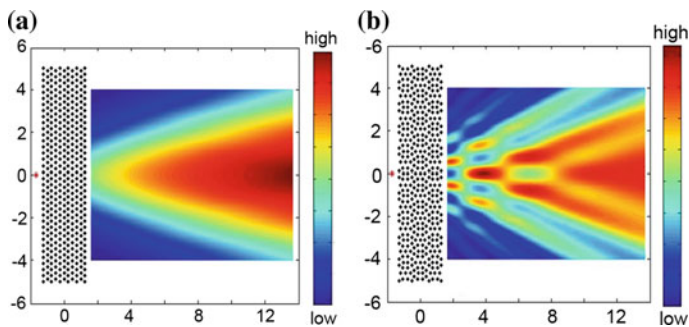

Fig. 15.21 Electric field intensity map of a cross-sectional view of the 2D source–image system when imaging by a photonic crystal flat lens consisting of ordered metallized TiO_2 nanotubes (**a**) and of a superlattice of optimized clusters (**b**)

The prospects for the elaboration of photonic crystal lenses and beam splitters on the basis of two-dimensional metallo-semiconductor structures prepared on porous templates and tubular structures have been also demonstrated on the instance of ZnSe templates [64]. The calculations performed for flat lenses assembled from metallized ZnSe tubes have proved again that focusing properties are better for lenses assembled from superlattices of optimized clusters as compared to those assembled from metallized ZnSe pores ordered in a triangular-lattice. The results of simulations for clusters consisting of metallized ZnSe tubes with parameters indicated in Table 15.1 are shown in Fig. 15.22.

Note that a clear superlensing effect is observed in this case (see Fig. 15.22), i.e., $S/\lambda^2 < 1$. The circles in Fig. 15.22 represent an area with the diameter equal to the wavelength of radiation. As one can see from Fig. 15.22b, these lenses can be used both for focusing or splitting the radiation. Unfortunately, the preparation of ZnSe

Table 15.1 The parameters of two samples assembled from metallized ZnSe tubes

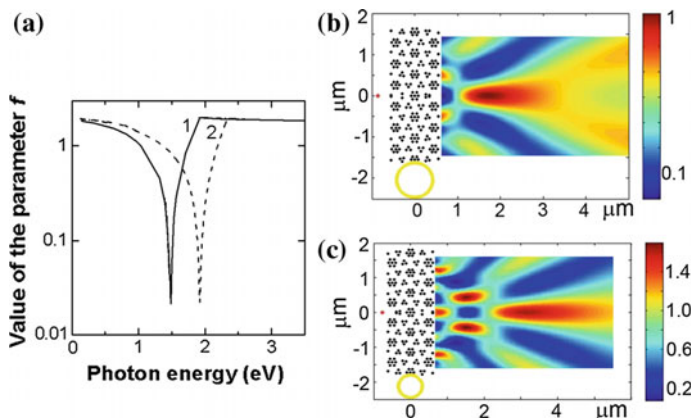| Sample	Inner diameter (nm)	Outer diameter (nm)	Distance between cylinder axis (nm)	Metal film thickness (nm)
#1	40	80	80	6
#2	50	100	100	21

Fig. 15.22 Spectral dependence of the parameter f for the sample #1 and #2 (**a**). Electric field intensity map of a cross-sectional view of the 2D source-image system when imaging by a photonic crystal flat lens consisting of clusters of metallized ZnSe nanotubes with parameters indicated in Table 15.1 for sample #1 at the photon energy of 1.48 eV (**b**), and for sample #2 at the photon energy of 1.92 (eV) (**c**)

structures with such morphologies is more complicated from the technological point of view.

A fascinating property of metallized semiconductor templates with ordered arrays of pores from the point of view of photonic applications is the possibility of their cleavage, as discussed in the previous section of the chapter.

Since metallized pores are parallel to the plane of cleavage, both TM and TE polarizations (with the E-field or H-field polarized in the direction of pore axis, respectively) can be easily realized. This is an important advantage as compared to pores oriented perpendicularly to the sample surface, where both the E-field and H-field are always perpendicular to the pore axis for a normally incident light. It was previously shown that photonic crystals exhibiting a photonic bandgap in both TE and TM polarizations are particularly interesting for a better control of light confinement [77].

To avoid the need of cleavage, technological methods have been developed for the preparation of templates with pores oriented parallel to the top surface of the substrate [64]. As shown in Fig. 15.23a, a design was used where some areas of the front surface of the substrate are covered by a photoresist, while other areas are
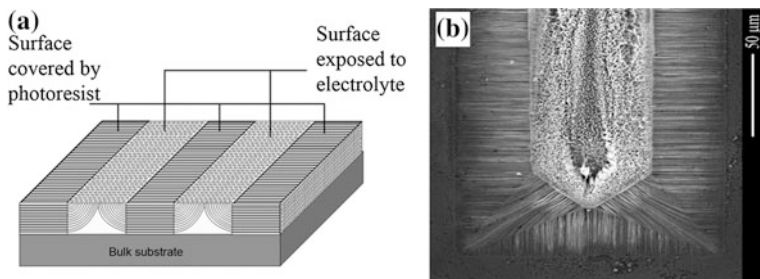
Fig. 15.23 **a** Illustration of the approach for the preparation of porous templates with pores parallel to the *top* surface of the sample. **b** Pt nanotubes deposited in an InP template with pores parallel to the *top* surface

exposed to the electrolyte in the electrochemical etching process. In this case, it is expected that the pores will grow from the surface exposed to the electrolyte initially in a direction perpendicular to the surface. However, with further propagation of pores, they will be deflected in directions parallel to the top surface, and will grow under the regions covered by the photoresist. These nanotemplates are suitable for the electrochemical deposition of metals inside pores, similar to the nanotemplates with pores perpendicular to the surface of the sample. Such kind of InP nanotemplate with Pt nanotubes deposited inside pores is shown in Fig. 15.23b. This approach is also suitable for the preparation of ZnSe templates and composites with pores parallel to the surface.

In a wider context, a range of industries can benefit from the development of metallo-dielectric composites such as transport industry (from the integration in magnetic sensors and radars), telecommunications (from systems of absorption of microwaves), energy sector (from the development of solar cells and fuel cells), as well as the health sector. The electro-deposition offers many advantages in the development of magnetic recording media as compared to other nano-technique, such as Electron Beam Lithography (EBL), Focus ion Beam System (FIB) and Nano-imprint. The dilemma between the grain size of the recording media and the coercivity is the main concern in the development of high information density magnetic recording media. The above mentioned technologies can meet the need of controllable grain size at very high cost. However, even at such cost the nano-fabrication is still not stable for the grain size under and below 100 nm. On the other hand, electro-deposition offers low cost and easy fabrication of nanowires and nanotubes below 100 nm. It is one of few methods that can overcome the geometrical restrictions of inserting metals into very deep nanometric cavities. As compared to nanowires, the interaction between array elements is significantly reduced in nanotubes by controlling the length of nanotubes and wall thickness, resulting in the formation of vortex domain wall in the nanotube arrays. Therefore, nanotubes offer great possibilities for improving the recording density.

Another field of applications of nanotubes and nanowires refers to biomagnetics, such as applications including molecular and cell separation [78–80], drug-delivery

systems [81, 82], biosensing [83–85], studies of cellular function [86, 87], as well as a variety of potential medical and therapeutic applications [86]. Scaffolds made of biodegradable nanowires have been used to repair brain damage and vision in animals, or coax neurons into forming engineered patterns [88, 89].

15.7 Conclusions

This review reveals the importance of nanotemplated growth of nanowires and nanotubes for nanofabrication. Nanowires are easier produced in nanotemplates as compared to nanotubes. However, nanotubes offer a series of advantages for applications. A comparative analysis of various templates evidenced their specific advantages and drawbacks. Basically three types of templates are used: ion-track membranes, porous alumina templates, and porous semiconductor templates. The ion-track membranes produced by bombarding thin polymeric films with heavy energetic ions followed by chemical etching offer advantages of producing nano-pores with desired shape and desired density controlled in a wide range over very large surfaces. Cylindrical, conical or double conical pores can be produced in polymeric membranes by choosing two parameters: the bulk etch rate (etching rate for non-irradiated material) and the track etch rate (the etching rate along the ion track). The main drawback of the ion-track membranes is related to employment of very large size and energy consuming equipment, such as ion accelerator, for the preparation of ultra-small structures such as nanowires or nanotubes.

As concerns alumina templates, apart from the advantage of excluding the need of using an ion accelerator, they have many other advantages over the polymeric membranes, such as high pore density, thermal stability, cost effectiveness and versatility. Pore diameter, length, inter-pore spacing, and pore ordering can be easily tailored in alumina templates by tuning the anodizing parameters such as voltage, time, electrolytes, pH value, and temperature. One of the most important advantages of porous alumina templates is associated with self-organization phe-nomena occurring during electrochemical anodization which results in the pro-duction of a hexagonal ordered morphology of pores. Highly ordered pores are usually obtained with a two-step anodization, textures being formed on the Al surface during the first anodization step, while the ordering of pores occurs in the second anodization step. However, ordered pores can also be obtained with one step anodization process performed under specific conditions.

Porous semiconductor templates have attracted considerable interest from the point of view of manufacturing conductive nanotemplates, since both porous alu-mina and etched ion track membranes have high resistivity, and often play a passive role in nanofabrication. The success with the implementation of porous semicon-ductor templates in nanofabrication is partially ensured by self-organization phe-nomena which occur also in semiconductor substrates during anodization, single crystalline two-dimensional hexagonal arrays of pores being formed. The con-ductivity of semiconductor templates is their major advantage over porous alumina

and etched ion track templates, which requires additional technological steps e.g. chemical modification of the inner surface of the pores prior to electrodeposition which leads to the incorporation of spurious phases in the produced nanotube walls.

Electrochemical and electroless deposition are the main methods user for producing metal nanostructures in all kinds of templates. Electrochemical deposition in etched ion track membranes leads in most of the cases to rod-like structures, while electroless deposition can be used for the preparation of hollow structures. Therefore, it is suitable for the production of nanotubes, since the deposition takes place only on the catalytic surface. To create a large number of catalytic nuclei on the surface, a three step process is employed with a preactivation, and an activation deposition. In spite of the fact that the electrodeposition process of metal only along the pore walls is not sufficiently controlled relative to an electroless plating method, it is in some cases suitable for the production of both metal nanowires and nanotubes by controlling the initial stages of electrochemical growth.

Several kinds of electrochemical deposition methods are applied for filling the pores of porous alumina templates, such as direct current electrodeposition, pulse electrodeposition, and alternating current electrodeposition. Different mechanisms have been proposed for the growth of nanotubes in alumina templates by electrodeposition. According to one of these mechanisms, the morphology of nanostructures produced into porous alumina template is determined by two parameters: growth rate parallel to current direction and growth rate perpendicular to current direction. At low current density, when these rates are nearly equal each other, wirelike 1D nanostructures are obtained. At high current density, the growth direction parallel to the current direction is the preferential one, and tubular structures are generated. According to another mechanism, the growth of metal nanotubes along the pore walls takes place by means of metallic nanoparticles immobilized on the wall surfaces, where the deposition interface moves from one isolated nanoparticle to another one via the dynamically created conducting paths.

Pulse electrodeposition proved to be the most appropriate method for preparation of nanotubes into porous semiconductor templates. It was found that under pulsed voltage regime it is possible to control the metal deposition within limited regions in depth of the porous structures by changing the ratio between the pulse duration and delay time between pulses. A uniform metal deposition inside the pores of the template can be attained by optimizing this parameter, therefore metal tubes with smooth walls of well controlled thickness and rather good mechanical strength being produced.

In semiconductor templates with ordered arrays of pores, it was found that packs of rows of metal nanotubes can be easily cleaved from the sample, and the possibility of such a cleavage is important from the point of view of photonic applications of the produces metallized porous semiconductor templates. The importance of semiconductor nanotemplates with metal nanotubes grown inside the pores for photonic applications was demonstrated by calculations of some photonic properties. The prospects of such metal/semiconductor nanocomposited for the development of beam splitters and focusing elements with a clear superlensing effect have been demonstrated.

Among other application of nanomaterials based on porous nanotemplates, their use in electronics, energy sector, optics, computers and communications, magnetism or biomedical sciences have been demonstrated. In particular, the electro-deposition proved to offer many advantages in the development of magnetic recording media and biomagnetics, such as applications including molecular and cell separation, drug-delivery systems, biosensing, studies of cellular function and therapeutics.

References

1. C.R. Martin, Nanomaterials, a membrane—based synthetic approach. Science **266**, 1961 (1994)
2. A. Fert, L. Piraux, Magnetic nanowires. J. Magn. Magn. Mater. **200**, 338 (1999)
3. I. Enculescu, Z. Siwy, D. Dobrev, C. Trautmann, M.E. Toimil Molares, R. Neumann, K. Hjort, L. Westerberg, R. Spohr. Copper nanowires electrodeposited in etched single-ion track templates. Appl. Phys. A **77**, 751 (2003)
4. I. Enculescu, Nanowires and nanotubes prepared using iob track membrane templates. Digest J. Nanomater. Biostruct. **1**(1), 15–20 (2006)
5. P. Lehana, S. Khan, S. Arya, Int. J. VLSI Signal. Proc. Appl. **1**, 32 (2011)
6. J. Lee, P. Lee, H. Lee, D. Lee, S.S. Lee, S.H. Ko, Nanoscale **4**, 6408 (2012)
7. P.-C. Hsu, S. Wang, H. Wu, V.K. Narasimhan, D. Kong, H.R. Lee, Y. Cui, Nat. Commun. **4**, 2522 (2013)
8. D.A. Dinh, K.N. Hui, K.S. Hui, P. Kumar, J. Singh. Rev. Adv. Sci. Eng. **2**, 324 (2013)
9. Y. Zhang, W. Xu, S. Xu, G. Fei, Y. Xiao, J. Hu, Nanoscale Res. Lett. **7**, 569 (2012)
10. G. Hrkac, J. Dean, D.A. Allwood, Phil. Trans. Phil. Trans. R. Soc. **A369**, 3214 (2011)
11. Y. Bian, Z. Cheng, X. Zhao, L. Liu, Y. Su, J. Xiao, J. Liu, J. Zhu, T. Zhou, J. Lightwave Technol. **31**, 1973 (2013)
12. W.L. Barnes, A. Dereux, T.W. Ebbesen, Nature **424**, 824 (2003)
13. Ch. Valsecchi, Al. G. Brolo. *Langmuir* **29**, 5638 (2013)
14. D.A. Bussian, S.A. Crooker, M. Yin, M. Brynda, Al. L. Efros, V.I. Klimov. Nat. Mater. **8**, 35 (2008)
15. V.A. Vlaskin, R.G. Beaulac, R. Daniel, Nano Lett. **9**, 4376 (2009)
16. M.E. Toimil Molares, V. Buschmann, D. Dobrev, R. Neumann, R. Scholz, I.U. Schuchert, J. Vetter. Single-crystalline copper nanowires produced by electrochemical deposition in polymeric ion track membranes. Adv. Mater. **13**, 62 (2001)
17. T. Ohgai, I. Enculescu, C. Zet, L. Westerberg, K. Hjort, R. Spohr, R. Neumann, J. Appl. Electrochem. **36**, 1157 (2006)
18. W. Schwarzacher, O.I. Kasyutich, P.R. Evans, M.G. Darbyshire, G. Yi, V.M. Fedosyuk, F. Rousseaux, E. Cambril, D. Decanini. J. Magn. Magn. Mater. **198–199**, 185 (1999)
19. L. Gravier, A. Fabian, A. Rudolf, A. Cachin, K. Hjort, J-Ph Ansermet, Meas. Sci. Tech. **15**, 420 (2004)
20. M. Sima, I. Enculescu, T. Visan, R. Spohr, C. Trautmann. Mol. Cryst. Liquid Cryst. **418**, 21 (749) (2004)
21. M. Sima, I. Enculescu, E. Vasile, J. Optoelectron. Adv. Mater. **8**, 825 (2006)
22. T. Ohgai, L. Gravier, X. Hoffer, J-Ph Ansermet, J. Appl. Electrochem. **35**, 479 (2005)
23. D. Xu, Y. Xu, D. Chen, G. Guo, L. Gui, Y. Tang, Chem. Phys. Lett. **325**, 340 (2000)
24. K. Nielsch, F. Müller, A. Li, U. Gösele, Uniform nickel deposition into ordered alumina pores by pulsed electrodeposition. Adv. Mater. **12**, 582 (2000)

25. I.U. Schuchert, M.E. Toimil Molares, D. Dobrev, J. Vetter, R. Neumann, M. Martin. J. Electrochem. Soc. **150**, C189 (2003)
26. W. Lee, R. Scholz, K. Nielsch, U. Gosele, Angew. Chem. Int. Ed. **44**, 6050 (2005)
27. G. Sharma, M.V. Pishko, C.A. Grimes, Fabrication of metallic nanowire arrays by electrodeposition into nanoporous alumina membranes: effect of barrier layer. J. Mater. Sci. **42**, 4738–4744 (2007)
28. M. Motoyama, Y. Fukunaka, T. Sakka, Y.H. Ogata. Electrochim. Acta **53**, 205 (20057)
29. E. Ferain, R. Legras. Heavy ion tracks in polycarbonate. Comparison with a heavy ion irradiated model compound (diphenyl carbonate). Nucl. Instrum. Meth. B **82**, 539–548 (1993)
30. E. Ferain, R. Legras, Track-etched membrane: dynamics of pore formation. Nucl. Instrum. Meth. B **84**, 331–336 (1994)
31. B. Bercu, I. Enculescu, R. Spohr, Nucl. Instrum. Meth. Phys. B **225**, 497 (2004)
32. I. Enculescu, M. Sima, M. Enculescu, E. Matei, M.E. Toimil Molares, Th. Cornelius. Nickel nanotubes prepared by electroless deposition in ion track templates. Optoelectr. Adv. Mater. Rapid Commun. **2**, 133–136 (2008)
33. H. Masuda, K. Fukuda, Ordered metal nanohole arrays made by a two-step replication of honeycomb structures of anodic alumina. Science **268**, 1466–1468 (1995)
34. G. Ali, M. Ahmad, J.I. Akhter, M. Maqbool, S.O. Cho, Novel structure formation in porous anodic alumina fabricated by single step anodization process. Micron **41**, 560–564 (2010)
35. G. Ali, M. Maqboo, Fabrication of cobalt-nickel binary nanowires in a highly ordered alumina template via AC electrodeposition. Nanoscale Res. Lett. **8**, 352 (2013)
36. S. Shamaila, R. Sharif, S. Riaz, M. Khaleeq-ur-Rahman, X.F. Han. Fabrication and magnetic characterization of Co_xPt_{1-X} nanowire arrays. Appl. Phys. A. **92**, 687–691 (2008)
37. S. Shamaila, R. Sharif, S. Riaz, M. Ma, M. Khaleeq-ur-Rahman, X.F. Han, Magnetic and magnetization properties of electrodeposited fcc CoPt nanowire arrays. J. Magn. Magn. Mater. **320**, 1803–1809 (2008)
38. S. Shamaila, R. Sharif, J.Y. Chen, H.R. Liu, X.F. Han, X.F. Magnetic, Field annealing dependent magnetic properties of $Co_{1-x}Pt_x$ nanowire arrays. J. Magn. Magn. Mater. **321**, 3984–3989 (2009)
39. R. Sharif, X.Q. Zhang, S. Shamaila, S. Riaz, L.X. Jiang, X.F. Han. Magnetic and magnetization properties of CoFeB nanowires. J. Magn. Magn. Mater. **310**, e830–e832 (2007)
40. H. Masuda, H. Yamada, M. Satoh, H. Asoh, Appl. Phys. Lett. **71**, 2770 (1997)
41. C.L. Chen, Y.-Y. Chen, S.-J. Lin, J.C. Ho, P.-C. Lee, C.-D. Chen, S.R. Harutyunyan, Fabrication and characterization of electrodeposited bismuth telluride films and nanowires. J. Phys. Chem. C **114**, 3385–3389 (2010)
42. R. Inguanta, M. Butera, C. Sunseri, S. Piazza, Fabrication of metal nano-structures using anodic alumina membranes grown in phosphoric acid solution: tailoring template morphology. Appl. Surf. Sci. **253**, 5447–5456 (2007)
43. K. Shimizu, K. Kobayashi, G.E. Thompson, G.C. Wood, Philos. Mag. A **66**, 643–652 (1992)
44. H. Fujikura, A. Liu, A. Hamamatsu, T. Sato, H. Hasegawa, Jpn. J. Appl. Phys. **39**, 4616 (2000)
45. T. Hirano, A. Ito, T. Sato, F. Ishikawa, H. Hasegawa, Jpn. J. Appl. Phys. **41**, 977 (2002)
46. H. Föll, S. Langa, J. Carstensen, M. Christophersen, I.M. Tiginyanu, Adv. Mater. **15**, 183 (2003)
47. H. Tsuchiya, M. Hueppe, T. Djenizian, P. Schmuki, Surf. Sci. **547**, 268 (2003)
48. S. Langa, M. Christophersen, J. Carstensen, I.M. Tiginyanu, H. Föll, Phys. Status Solidi A **197**, 77 (2003)
49. I.M. Tiginyanu, E. Monaico, V.V. Ursaki, V.E. Tezlevan, R.W. Boyd, Appl. Phys. Lett. **86**, 063115 (2005)
50. I.M. Tiginyanu, E. Monaico, V.V. Ursaki, E. Foca, H. Föll, Electrochem. Solid State Lett. **10**, D127 (2007)
51. I. Tiginyanu, E. Monaico, E. Monaico, Ordered arrays of metal nanotubes in semiconductor envelope. Electrochem. Commun. **10**, 731 (2008)

52. M.E. Toimil Molares, N. Chtanko, T.W. Cornelius, D. Dobrev, I. Enculescu, R.H. Blick, R. Neumann. Fabrication and contacting of single Bi nanowires. Nanotechnology **15**, S 201–S 207 (2004)
53. M. Sima, I. Enculescu, C. Trautmann, R. Neumann, Electrodeposition of CdTe nanorods in ion track membranes. J. Optoelectron. Adv. Mater. **6**, 121–125 (2004)
54. G.E. Possin, Forming very small diameter wires. Rev. Sci. Instrum. **41**, 772 (1970)
55. G.E. Possin. Superconductivity in nearly one-dimensional tin wires. Physica (Utrecht) **55**, 339 (1971)
56. D.T. Mitchell, S.B. Lee, L. Trofin, N. Li, T.K. Nevanen, H. Soderlund, C.R. Martin, J. Am. Chem. Soc. **124**, 11864 (2002)
57. D. Routkevitch, J. Chan, J.M. Xu, M. Moskovits, Electrochem. Soc. Proc. Ser. PV **350**, 97 (1997)
58. A.J. Yin, J. Li, W. Jian, A.J. Bennett, J.M. Xu, Fabrication of highly ordered metallic nanowire arrays by electrodeposition. Appl. Phys. Lett. **79**, 1039 (2001)
59. H. Cao, L. Wang, Y. Qiu, Q. Wu, G. Wang, L. Zhang, X. Liu, Generation and growth mechanism of metal (Fe Co, Ni) nanotube arrays. ChemPhysChem **7**, 1500–1504 (2006)
60. W.-C. You, J.-K. Lee, Field-dependent growth patterns of metals electroplated in nanoporous alumina membranes. Adv. Mater. **16**, 1097–1101 (2004)
61. W. Lee, R. Scholz, K. Nielsch, U. Gosele, A template-based electrochemical method for the synthesis of multisegmented metallic nanotubes. Angew. Chem. **117**, 6204–6208 (2005)
62. D.D. Sung, M.S. Choo, J.S. Noh, W.B. Chin, W.S. Yang, A new fabrication method of aluminum nanotube using anodic porous alumina film as a template. Bull. Korean Chem. Soc. **27**, 1159 (2006)
63. G.N. Ivanova, D.D. Nedeoglo, N.D. Negeoglo, V.P. Sirkeli, I.M. Tiginyanu, V.V. Ursaki, J. Appl. Phys. **101**, 063543 (2007)
64. I.M. Tiginyanu, V.V. Ursaki, E. Monaico, M. Enachi, V.V. Sergentu, G. Colibaba, D.D. Nedeoglo, A. Cojocaru, H. Föll, Quasi-ordered networks of metal nanotubes embedded in semiconductor matrices for photonic applications. J. Nanoelectr. Optoelectr. **6**, 463–472 (2011)
65. I. Tiginyanu, E. Monaico, V. Sergentu, A. Tiron, V. Ursaki, Metallized porous GaP templates for electronic and photonic applications. ECS J. Solid State Sci. Technol. **4**, P57–P62 (2015)
66. D. Vanmaekelbergh, A. Koster, F.I. Marin, Adv. Mater. **9**, 575 (1997)
67. M. Scalora, G. D'Aguanno, N. Mattiucci, M.J. Bloemer, D. de Ceglia, M. Centini, A. Mandatori, C. Sibilia, N. Akozbek, M.G. Cappeddu, M. Fowler, J.W. Haus, Opt. Express **15**, 508 (2007)
68. M. Bloemer, G. D'Aguanno, M. Scalora, N. Mattiucci, D. de Ceglia, Opt. Express **16**, 19342 (2008)
69. J.B. Pendry, Negative refraction makes a perfect lens. Phys. Rev. Lett. **85**, 3966 (2000)
70. D.R. Smith, W.J. Padilla, D.C. Vier, S.C. Nemat-Nasser, S. Schultz, Composite medium with simultaneously negative permeability and permittivity. Phys. Rev. Lett. **84**, 4184 (2000)
71. L.-M. Li, Z.-Q. Zhang, Multiple-scattering approach to finite-sized photonic band-gap materials. Phys. Rev. B **58**, 9587 (1998)
72. V.V. Sergentu, I.M. Tiginyanu, V.V. Ursaki, M. Enachi, S.P. Albu, P. Schmuki. Negative index material lenses based on metallo-dielectric nanotubes. Phys. Stat. Sol. (RRL) **2**, 242 (2008)
73. M. Hofman, G. Scherrer, M. Kadic, X. Melique, W. Smigaj, B. Cluzel, S. Guenneau, D. Lippens, F. de Fornel, B. Gralak, O. Vanbesien, J. Nanomed. Nanotechnol. **4**, 1000185 (2013)
74. G. Scherrer, M. Hofman, W. Smigaj, M. Kadic, T.M. Chang, X. Melique, D. Lippens, O. Vanbesien, B. Cluzel, F. de Fornel, S. Guenneau, B. Gralak, Phys. Rev. B **88**, 115110 (2013)
75. M. Hofman, D. Lippens, O. Vanbesien, Appl. Opt. **49**, 5806 (2010)
76. M. Enachi, I. Tiginyanu, V. Sprincean, V. Ursaki, Self-organized nucleation layer for the formation of ordered arrays of double-walled TiO_2 nanotubes with temperature controlled inner diameter. Phys. Status Solidi RRL **4**, 100–102 (2010)
77. F. Wen, S. David, X. Checoury, M. El Kurdi, P. Boucaud, Opt. Express **16**, 12278 (2008)

78. L.R. Moore, M. Zborowski, L. Sun, J.J. Chalmers, J. Biochem. Biophys. Methods **37**, 11 (1998)
79. J. Escrig, P. Landeros, D. Altbir, E.E. Vogel, J. Magn. Magn. Mater. **310**, 2448 (2007)
80. S.B. Lee, D.T. Mitchell, L. Trofin, T.K. Nevanen, H. Sderlund, C.R. Martin, Science **296**, 2198 (2002)
81. C.R. Martin, P. Kohli, Nat. Rev. Drug Discov. **2**, 29 (2003)
82. H. Hillebrenner, F. Buyukserin, J.D. Stewar, C.R. Martin, Nanomedicine **1**, 39 (2006)
83. D.R. Baselt, G.L. Lee, M. Natesan, S.W. Metzger, P.E. Sheehan, R.J. Colton. Biosens. Bioelectron. **13**, 731 (1998)
84. R. Fan, R. Karnik, M. Yue, D. Li, A. Majumdar, P. Yang, Nano Lett. **5**, 1633 (2005)
85. P. Ball. Nanowire sensors pass drugs test. Nat. Nanozone News (2005)
86. F.J. Alenghat, B. Fabry, K.Y. Tsai, W.H. Goldmann, D.E. Ingber, Biochem. Biophys. Res. Commun. **277**, 93 (2000)
87. R.J. Mannix, S. Kumar, F. Cassiola, M. Montoya-Zavala, E. Feinstein, M. Prentiss, D.E. Ingber, Nature Nanotech. **3**, 36 (2008)
88. K. Bullis, Technol. Rev. **109**, 16 (2006)
89. R.R. Llinas, K.D. Walton, M. Nakao, I. Hunter, P.A. Anquetil, Neuro-vascular central nervous recording/stimulating system: using nanotechnology probes. J. Nanoparticle Res. **7**, 111–127 (2005)